J|A|C|S
ARTICLES
Published on Web 04/17/2002

Spectroscopic Properties of Tyrosyl Radicals in Dipeptides

Idelisa Ayala,[†] Kevin Range,[‡] Darrin York,[‡] and Bridgette A. Barry*[,†]

Contribution from the Department of Biochemistry, Molecular Biology, and Biophysics, University of Minnesota, 1479 Gortner Avenue, St. Paul, Minnesota 55108-1022, and Department of Chemistry, University of Minnesota, Minneapolis, Minnesota 55455-0431

Received June 15, 2001

Abstract: Redox-active tyrosine residues play important roles in long-distance electron reactions in enzymes, including prostaglandin H synthase, galactose oxidase, ribonucleotide reductase, and photosystem II. Magnetic resonance and vibrational spectroscopy provide methods with which to study the structures of redox-active amino acids in proteins. In this report, ultraviolet photolysis was used to generate tyrosyl radicals from polycrystalline tyrosinate or dipeptides, and the structure of the radical was investigated with EPR and reaction-induced FT-IR spectroscopy at 77 K. Photolysis at 77 K is expected to generate a neutral tyrosyl radical through oxidation of the aromatic ring. EPR and FT-IR results obtained from ^{13}C-labeled tyrosine were consistent with that expectation. Surprisingly, labeling of the tyrosyl amino group with ^{15}N also resulted in isotope-shifted bands in the photolysis spectrum. The force constant of a NH deformation mode increased when the tyrosyl radical was generated. These data suggest an interaction between the π system of the tyrosyl radical and the amino group. In spectra acquired from the dipeptides, evidence for a sequence-dependent interaction between the tyrosyl radical and the amide bond of the dipeptide was also obtained. We postulate that perturbation of the amino or the amide/imide groups may occur through a spin polarization mechanism, which is indirectly detected as a change in NH force constant. This conclusion is supported by density functional calculations, which suggest a conformationally sensitive delocalization of spin density onto the amino and carboxylate groups of the tyrosyl radical. These experiments provide a step toward a detailed spectral interpretation for protein-based tyrosyl radicals.

Tyrosyl radicals are postulated to mediate long-distance electron-transfer reactions in a number of enzymes, including prostaglandin H synthase,[1] galactose oxidase,[2] ribonucleotide reductase,[3] and photosystem II.[4] The environmental factors responsible for functional control of these redox-active species have not as yet been elucidated. Optical and magnetic resonance spectroscopies have been used to determine the structure of tyrosyl and phenoxyl radicals produced in tyrosinate and phenolate solutions {for examples, see refs 5−12}. Vibrational spectroscopy has been applied to the determination of the ground-state structure for peptides {for examples, see refs 13−19}. However, there have been few[20,21] reported vibrational and EPR studies of tyrosyl radical structures in peptides, which serve to model some aspects of the protein environment.

Tyrosyl radicals can be generated by ultraviolet photolysis of alkaline, polycrystalline tyrosine.[11] This procedure generates a neutral radical in which spin density is located on carbons 1′, 3′, and 5′ and on the phenolic oxygen (Figure 1A).[6,7,9,11,12,22,23] The EPR line shape is dependent on the details of this spin density distribution and on the dihedral angle (θ) at the $C_\beta-C_1'$ bond. Interestingly, although a distribution of three different $C_\beta-C_1'$ conformers is expected in tyrosinate solutions,[24] the EPR

* Author for correspondence. Telephone: 612-624-6732. Fax: 612-625-5780. E-mail: barry@biosci.cbs.umn.edu.
[†] University of Minnesota, St. Paul.
[‡] University of Minnesota, Minneapolis.

(1) Smith, W. L.; Eling, T. E.; Kulmacz, R. J.; Marnett, L. J.; Tsai, A.-L. *Biochemistry* **1992**, *31*, 3−7.
(2) Whittaker, M. M.; Whittaker, J. W. *J. Biol. Chem.* **1990**, *265*, 9610−9613.
(3) Larsson, A.; Sjoberg, B.-M. *EMBO* **1986**, *5*, 2037−2040.
(4) Barry, B. A.; Babcock, G. T. *Proc. Natl. Acad. Sci. U.S.A.* **1987**, *84*, 7099−7103.
(5) Fasanella, E. L.; Gordy, W. *Proc. Natl. Acad. Sci. U.S.A.* **1969**, *62*, 299−304.
(6) Box, H. C.; Budzinski, E. E.; Freund, H. G. *J. Phys. Chem.* **1974**, *61*, 2222−2226.
(7) Dixon, W. T.; Moghimi, M.; Murphy, D. *J. Chem Soc. London, Faraday Trans. 2* **1974**, *70*, 1713−1720.
(8) Tripathi, G. N. R.; Schuler, R. H. *J. Chem. Phys.* **1984**, *81*, 113−121.
(9) Sealy, R. C.; Harman, L.; West, P. R.; Mason, R. P. *J. Am. Chem. Soc.* **1985**, *107*, 3401−3406.
(10) Johnson, C. R.; Ludwig, M.; Asher, S. A. *J. Am. Chem. Soc.* **1986**, *108*, 905−912.
(11) Barry, B. A.; El-Deeb, M. K.; Sandusky, P. O.; Babcock, G. T. *J. Biol. Chem.* **1990**, *265*, 20139−20143.
(12) Hulsebosch, R. J.; van der Brink, J. S.; Nieuwenhuis, S. A. M.; Gast, P.; Raap, J.; Lugtenburg, J.; Hoff, A. J. *J. Am. Chem. Soc.* **1997**, *119*, 8685−8694.
(13) Qian, W.; Bandekar, J.; Krimm, S. *Biopolymers* **1991**, *31*, 193−210.
(14) Eberhardt, E. S.; Raines, R. T. *J. Am. Chem. Soc.* **1994**, *116*, 2149−2150.
(15) Farkas, Ö.; McAllister, M. A.; Ma, J. H.; Perczel, A.; Hollósi, M.; Csizmadia, I. G. *J. Mol. Struct.* **1996**, *369*, 105−114.
(16) Torii, H.; Tasumi, M. *J. Raman Spectrosc.* **1998**, *29*, 81−86.
(17) Kocak, A.; Luque, R.; Diem, M. *Biopolymers* **1998**, *46*, 455−463.
(18) Asplund, M. C.; Zanni, M. T.; Hochstrasser, R. M. *Proc. Natl. Acad. Sci. U.S.A.* **2000**, *97*, 8219−8224.
(19) Bour, P.; Kubelka, J.; Keiderling, T. A. *Biopolymers* **2000**, *53*, 380−395.
(20) Bent, D. V.; Hayon, E. *J. Am. Chem. Soc.* **1975**, *97*, 2599−2619.
(21) Tanner, C.; Navaratnam, S.; Parsons, B. J. *Free Radical Biol. Med.* **1998**, *24*, 671−678.
(22) Nwobi, O.; Higgins, J.; Zhou, X.; Liu, R. *Chem. Phys. Lett.* **1997**, *272*, 155−161.
(23) Wise, K. E.; Pate, J. B.; Wheeler, R. A. *J. Phys. Chem. B* **1999**, *103*, 4764−4772.
(24) Warncke, K.; Babcock, G. T.; McCracken, J. *J. Phys. Chem.* **1996**, *100*, 4654−4661.

10.1021/ja0164327 CCC: $22.00 **© 2002 American Chemical Society**

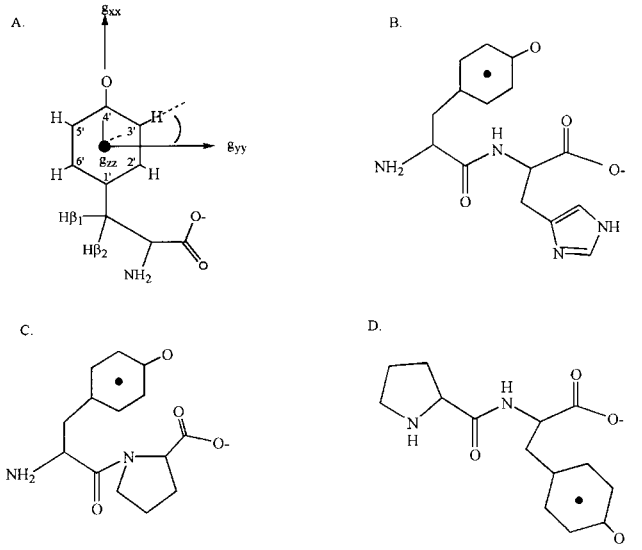

Figure 1. Structures and numbering of the tyrosyl radical (A). Structures of the tyr-his (B), tyr-pro (C), and pro-tyr (D) dipeptides. The axis system in part A shows the orientation of the *g* axis.

spectrum of the free radical produced from the polycrystalline state is consistent with a relatively narrow distribution of angles at the $C_\beta-C_1$ bond.[12,25]

In addition to magnetic resonance, vibrational spectroscopic techniques have been applied. Previous Raman vibrational studies have shown that formation of the radical is associated with perturbation of ring stretching vibrations and with a dramatic increase in the CO stretching frequency.[8,10,26,27]

Pulse radiolysis has been used to generate tyrosyl radicals in peptides. In one study of a his and tyr containing dipeptide (Figure 1B), evidence for migration of the unpaired electron from a histidine side chain to the tyrosine side chain on the microsecond time scale was obtained by time-resolved optical spectroscopy.[21] Dipeptides can exist in and sample over multiple conformational states in solution; the details of this conformational distribution are critically dependent on sequence.[17,28] The amide or, in the case of proline, imide bond is polar, and redistribution of electrons leads to partial negative charge on the nitrogen. Because the amide bond has double bond character, rotation about this bond is restricted. In dipeptides, the *trans* isomer is expected to be preferred. However, when the dipeptide contains an imide bond to a proline residue, for example, tyr-pro (Figure 1C), the *trans* form is destabilized relative to the *cis* isomer {see ref 29 and references therein}.

In this report, we describe EPR and vibrational studies of photolysis-generated radicals in tyrosine-containing dipeptides (for examples, see Figure 1B−D). These studies provide evidence for an interaction between the electron-deficient π system of the tyrosyl radical and the amino terminal groups. This is corroborated by tyrosine-containing dipeptide studies, which provide evidence for an interaction between the tyrosyl radical and the amide functional group. This interaction may occur through an intramolecular spin polarization effect[30] that is indirectly detected as a change in bond strength in the vibrational spectrum. This interpretation is supported by DFT calculations, which are discussed.

Materials and Methods

L-Tyrosine was purchased from Sigma (St. Louis, MO). L-Tyrosinephenol-*4*-^{13}C (99%) and L-tyrosine-^{15}N (95−99%) were from Cambridge Isotope Laboratories (Andover, MA). The tyrosine-containing dipeptides were from Bachem (King of Prussia, PA). Boric acid was from EM Science (Cherry Hill, NJ), and sodium borate from Mallinckrodt (Phillipsburg, NJ). A 100 mM solution of tyrosine, $^{13}C_1$ (4′-phenol) tyrosine, ^{15}N-tyrosine and tyrosine-containing dipeptides in 10 mM borate-NaOH, pH 11, was employed.

EPR spectroscopy was performed on a Bruker (Billerica, MA) EMX 6/1 X-band spectrometer with a Wilmad (Buena, NJ) variable-temperature dewar. EPR spectra were recorded at 77 K; the temperature was regulated by a stream of cold nitrogen. Illumination was provided by an Nd:YAG laser (Continuum, Santa Clara, CA), equipped with a fourth harmonic generator and producing 266 nm, 7 ns pulses. Samples were partially dehydrated in the quartz EPR tube and were flashed in the EPR cavity with five laser flashes at a frequency of 10 Hz and a pulse energy of 35−37 mJ. Spectral conditions were as follows: microwave frequency, 9.2 GHz; power, 0.2 mW; modulation amplitude, 2 G; modulation frequency, 100 kHz; scan time, 168 s; number of scans, 4; and time constant, 1.3 s. Data were obtained on two different samples and were averaged. Simulations of EPR spectra were performed using a computer program written by Hoganson and Babcock[31] and using parameters previously reported for tyrosyl radicals.[12] Igor Pro software (Lake Oswego, OR) was used for spectral manipulation and spin quantitation.

Reaction-induced FT-IR spectra were recorded on a Nicolet 60-SXR spectrometer equipped with a MCT-B detector (Nicolet, Madison, WI) and with a Hansen liquid nitrogen cryostat (R. G. Hansen & Associates, Santa Barbara, CA). Spectral conditions were as follows: resolution, 4 cm^{-1}; mirror velocity, 1.57 cm/s; apodization function, Happ-Genzel; levels of zero filling, one; data acquisition time, 1 min; and temperature, 77 K. Illumination was provided by an Nd:YAG laser at 266 nm (Continuum, Santa Clara, CA). Five laser flashes were employed with a frequency of 10 Hz and pulse energy of 35−37 mJ. The sample was partially dehydrated on a CaF_2 window. The UV spectrum (Hitachi, Danbury, CT) of the FT-IR sample was obtained, and the absorption band at 294 nm was used for normalization. The infrared bands either at 1500 cm^{-1} or at 1260 cm^{-1} were also used for normalization. The results obtained using all three methods were similar. Difference spectra, associated with the production of the radical, were constructed by subtracting data acquired before illumination from data acquired after illumination. Data were obtained on 2−8 different samples and were averaged.

Electronic structure calculations were performed on the tyrosyl radical using unrestricted density-functional theory (DFT). The three-parameter hybrid exchange functional of Becke[32] in conjunction with the correlation functional of Lee, Yang, and Parr[33] was used to model the exchange-correlation energy functional (B3LYP). Unrestricted density-functional calculations were performed with the 6-31++G-(d,p) basis set using GAUSSIAN98.[34] Geometry optimizations were performed based on the three local minima reported by Qin and Wheeler for the neutral tyrosyl radical.[35] The tyrosyl radical was chosen to have a neutral amino terminus and anionic carboxyl terminus, consistent with the expected ionized state at the experimental pH.

Results

EPR Spectroscopy of Tyrosyl Radicals. At 77 K, UV photolysis of an alkaline tyrosinate solution generated an EPR

(25) Warncke, K.; Perry, M. S. *Biochim. Biophys. Acta* **2001**, *1545*, 1−5.
(26) Takeuchi, H.; Watanabe, N.; Satoh, Y.; Harada, I. *J. Raman Spectrosc.* **1989**, *20*, 233−237.
(27) Mukherjee, A.; McGlashen, M. L.; Spiro, T. G. *J. Phys. Chem.* **1995**, *99*, 4912−4917.
(28) Kolaskar, A. S.; Sawant, S. *Int. J. Peptide Prot. Res.* **1996**, *47*, 110−116.
(29) Takeuchi, H.; Harada, I. *J. Raman Spectrosc.* **1990**, *21*, 509−515.
(30) Walden, S. E.; Wheeler, R. A. *J. Am. Chem. Soc.* **1997**, *119*, 3175−3176.
(31) Hoganson, C. W.; Babcock, G. T. *Biochemistry* **1992**, *31*, 11874−11880.
(32) Becke, A. D. *J. Chem. Phys.* **1993**, *98*, 5648−5652.
(33) Lee, C.; Yang, W.; Parr, R. G. *Phys. Rev. B* **1988**, *58*, 785−789.

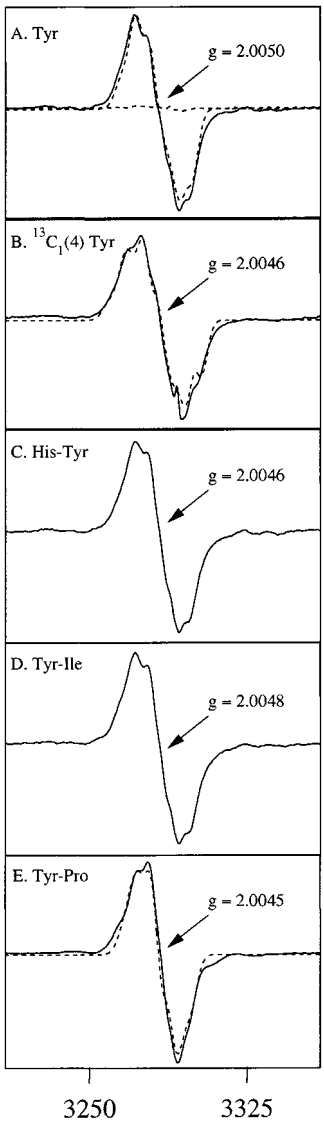

Figure 2. EPR spectra of tyrosyl radicals generated by UV photolysis of solutions containing (A) tyrosinate (solid line), (B) $^{13}C_1$(4′-phenol) tyrosinate (solid line), (C) his-tyr, (D) tyr-ile, and (E) tyr-pro (solid line). Simulations of the EPR spectra are shown as dashed lines in A, B, and E. The flat dotted line in part A shows the result of UV illumination on the borate buffer alone.

signal (Figure 2A, solid line), similar to spectra previously reported for a neutral tyrosyl radical.[11] The measured g value is 2.0050 ± 0.0001. The spectral broadening observed upon ^{13}C labeling of ring carbon 4 (Figure 1A) suggests that this EPR spectrum arises from a tyrosyl radical (Figure 2B), as does the lack of detectable signal after photolysis of borate buffer alone (Figure 2A, flat dotted line). The EPR line shapes and g values of the radical produced in his-tyr (g = 2.0046 ± 0.0001) and tyr-ile (g = 2.0048 ± 0.0001) peptides are similar (Figure 2C−D) to those observed in tyrosinate solutions. A minor perturbation of the EPR line shape was observed when a tyrosyl radical was produced in a tyr-pro dipeptide (Figure 2E, solid line), while the g value of this paramagnetic species was unchanged (g = 2.0045 ± 0.0001). The overall similarity of radical line shape and g value in the dipeptides and in the tyrosinate solution provides evidence that a neutral tyrosyl radical is produced in each case.

Table 1. EPR Simulation Parameters (g_{xx} = 2.0070, g_{yy} = 2.0046, g_{zz} = 2.0024; line width = 2.7; frequency = 9.21 GHz)[a]

hfi	A_{xx} (G)	A_{yy} (G)	A_{zz} (G)	A_{iso} (G)	ϕ
Tyr					
C2′-H	1.7	2.7	0.4	1.6	30
C3′-H	−9.6	−2.8	−7.0	−6.5	−23
C5′-H	−9.6	−2.8	−7.0	−6.5	23
C6′-H	1.7	2.7	0.4	1.6	−30
C1′-$H_{\beta1}$	0.62	0.58	0.58	0.59	0
C1′-$H_{\beta2}$	11.0	11.0	11.0	11.0	0
$^{13}C_1$(4′) Tyr					
C2′-H	1.7	2.7	0.4	1.6	30
C3′-H	−9.6	−2.8	−7.0	−6.5	−23
C5′-H	−9.6	−2.8	−7.0	−6.5	23
C6′-H	1.7	2.7	0.4	1.6	−30
C1′-$H_{\beta1}$	0.62	0.58	0.58	0.59	0
C1′-$H_{\beta2}$	11.0	11.0	11.0	11.0	0
4′-^{13}C	−11.5	−12.5	−7.0	−10.3	0
Tyr-Pro					
C2′-H	1.7	2.7	0.4	1.6	30
C3′-H	−9.8	−3.0	−7.2	−6.7	−23
C5′-H	−9.8	−3.0	−7.2	−6.7	23
C6′-H	1.7	2.7	0.4	1.6	−30
C1′-$H_{\beta1}$	2.1	1.9	1.9	2.0	0
C1′-$H_{\beta2}$	8.2	7.9	7.9	8.0	0

[a] EPR simulations were performed through the use of a computer program previously described.[31] Hyperfine interactions (hfi) were obtained from ref 12 with minor modifications and are given in Gauss. The Euler angle ϕ represents the in-plane rotation of the hyperfine component about the g_z and is defined as positive clockwise rotation (Figure 1A). Euler angles θ and ψ were set to zero. The average isotropic g value was obtained experimentally.

EPR simulations were performed for the signal derived by photolysis of tyrosinate (Figure 2A, dashed line), $^{13}C_1$ (4′-phenol) tyrosinate (Figure 2B, dashed line), and the tyr-pro dipeptide (Figure 2E, dashed line). The parameters employed are given in Table 1 and include significant couplings only to protons on the phenol ring and at the methylene position.[11,12] The spectra were fit with the same **g** tensor, derived to fit the average experimental isotropic g value (Table 1). Simulations of the tyrosyl and $^{13}C_1$ tyrosyl radical spectra were performed with a self-consistent set of parameters, except that for the ^{13}C isotopomer, addition of a hyperfine interaction with the ^{13}C nucleus and a small 3, 5 proton hyperfine tensor reorientation was included.[12] These successful simulations of tyrosyl and $^{13}C_1$ tyrosyl radical spectra with a consistent parameter set provide additional evidence that the detected radical arises from the tyrosyl phenol ring. Simulation of the tyr-pro EPR spectrum (Figure 2E, dashed line) indicates that changes in hyperfine splittings to the β-methylene protons can account for its EPR line shape. These alterations can be attributed to a proline-induced change in the lowest energy conformation of the tyrosine side chain. This alteration is consistent with an approximately 9° rotation at the $C_\beta-C_1'$ bond.

(34) Frisch, M. J.; Trucks, G. W.; Schlegel, H. B.; Scuseria, G. E.; Robb, M. A.; Cheeseman, J. R.; Zakrzewski, V. G.; Montgomery, J. A.; Stratmann, R. E.; Burant, J. C.; Dapprich, S.; Millam, J. M.; Daniels, A. D.; Kudin, K. M.; Strain, M. C.; Farkas, O.; Tomasi, J.; Barone, V.; Cossi, M.; Cammi, R.; Mennucci, B.; Pomelli, C.; Adamo, C.; Clifford, S.; Ochterski, J.; Petersson, G. A.; Ayala, Q.; Cui, P. Y.; Morokuma, K.; Malick, D. K.; Rabuck, A. D.; Raghavachari, K.; Foresman, J. B.; Cioslowski, J.; Ortiz, J. V.; Baboul, A. G.; Stefanov, B. B.; Liu, G.; Liashenko, A.; Piskorz, P.; Komaromi, I.; Gomperts, R.; Martin, R. L.; Fox, D. J.; Keith, T.; Al-Laham, M. A.; Peng, C. Y.; Nanayakkara, A.; Challacombe, M.; Gill, P. M. W.; Johnson, B.; Chen, W.; Wong, M. W.; Andres, J. L.; Gonzalez, M.; Head-Gordon, M.; Replogle, E. S.; Pople, J. A. *Gaussian 98*, Revision A.9; Gaussian, Inc.: Pittsburgh, PA, 1998.
(35) Qin, Y.; Wheeler, R. A. *J. Am. Chem. Soc.* **1995**, *117*, 6083−6092.

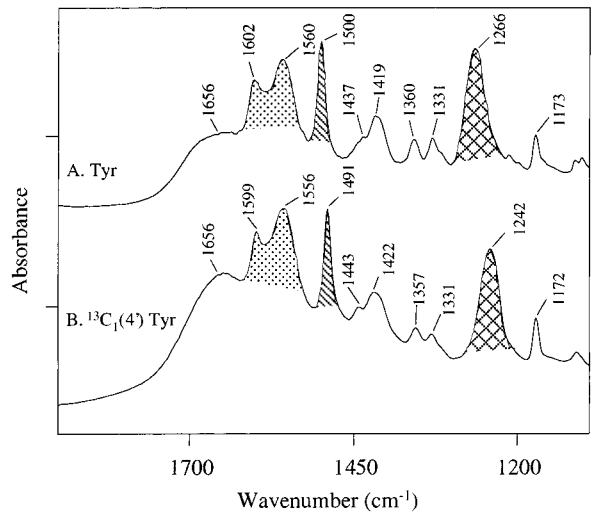

Figure 3. Ground-state FT-IR spectra of (A) tyrosinate and (B) $^{13}C_1$(4′-phenol) tyrosinate. Spectral contributions from the borate buffer were subtracted from these data. The tick marks on the *y*-axis represent 0.4 absorbance units. Crosshatched lines are assigned to ring modes and the CO stretching vibrations of tyrosinate.

Ground-State FT-IR Spectra of Tyrosinate. Figure 3 shows the ground-state FT-IR spectra of tyrosinate (A) and $^{13}C_1$(4′-phenol) tyrosinate (B). Borate buffer contributions were subtracted. In the tyrosinate FT-IR spectrum, a band is observed at 1266 cm^{-1} (Figure 3A). This spectral feature shifts to 1242 cm^{-1} ($\Delta = -24$ cm^{-1}) in $^{13}C_1$(4′-phenol) tyrosinate (Figure 3B). A downshifted line at 1238 cm^{-1} ($\Delta = -28$ cm^{-1}) is observed for $^{13}C_6$ (ring) tyrosinate, an isotopomer in which all the carbons of the ring are labeled with ^{13}C (data not shown). These are the magnitudes of the ^{13}C shift expected for a harmonic C−O stretching mode, and, therefore, we assign this band to the C−O ($\nu_{7a'}$) vibration of the tyrosinate species.[22,26,27,36] The CCH bending mode (υ_{9a}) is observed at 1173 cm^{-1} (Figure 3A) and is relatively insensitive to ^{13}C labeling (Figure 3B), as expected.[22,26,27,36]

A broad band at approximately 1650 cm^{-1} arises from residual water contributions to the spectrum[37] and also contains a less intense contribution from the NH bending mode of the amino group (Figure 1A) {see below). A band at 1602 cm^{-1} is observed in tyrosinate (Figure 3A), which downshifts to 1599 cm^{-1} ($\Delta = -3$ cm^{-1}) in the $^{13}C_1$(4′-phenol) tyrosinate (Figure 3B). In addition, a band at 1500 cm^{-1} downshifts to 1491 cm^{-1} ($\Delta = -9$ cm^{-1}) in $^{13}C_1$(4′-phenol) tyrosinate (Figure 3B). The 1602 and 1500 cm^{-1} bands are assigned to ring stretching modes, υ_{8a} and υ_{19a}, respectively, of the tyrosinate species; this assignment is based on the observed frequencies and the observed isotope shifts.[8,22,26,27,36]

Additional ring modes and CC/C−H modes are also expected in the tyrosinate FT-IR spectrum. For example, mode υ_{8b} (ring CC stretch) is expected at approximately 1550 cm^{-1}, and mode υ_{19b} (CC stretch/CH bend) is expected at approximately 1440 cm^{-1}.[27] In the tyrosinate spectrum (Figure 3A), vibrational lines with similar frequencies, 1560 and 1437 cm^{-1}, are observed. The 1560 cm^{-1} band is a ring stretching vibration, as evidenced by a downshift of 4 and 11 cm^{-1} in $^{13}C_1$(4′-phenol) tyrosinate (Figure 3B) and in $^{13}C_6$(ring) tyrosinate (data not shown), respectively. The asymmetric stretching vibration of the carboxylate group may also make a contribution in this spectral region. The 1437 cm^{-1} band did not show significant isotope-induced downshifts in ring-labeled isotopomers; this result is inconsistent with its assignment to υ_{19b}, but may be consistent with assignment to the symmetric carboxylate stretching vibration. Additional bands are observed at 1419, 1360, and 1331 cm^{-1} (Figure 3A). In $^{13}C_1$(4′-phenol) tyrosinate (Figure 3B), these lines are observed at 1422, 1357, and 1331 cm^{-1}. In $^{13}C_6$-(ring) tyrosinate (data not shown), these spectral features are observed at 1417, 1356, and 1329 cm^{-1}. Potential assignments for these spectral features are to the carboxylate group, the amino group and/or α and β carbons, or ring vibrational modes with small isotope shifts.

Ground-State FT-IR Spectra of Tyrosine-Containing Dipeptides. Figure 4 shows the ground-state FT-IR spectra of tyr-his (A), tyr-ile (B), tyr-pro (C), tyr-leu (D), his-tyr (E), ile-tyr (F), pro-tyr (G), and leu-tyr (H). The C−O band is observed between 1266 and 1269 cm^{-1} in the tyrosine-containing dipeptides (Figure 4A−H), and υ_{9a} is observed at 1172−1173 cm^{-1}(Figure 4A−H). The ring stretching vibrations, observed in tyrosine at 1602 and 1500 cm^{-1}, are present at frequencies between 1602 and 1600 cm^{-1} and 1501−1500 cm^{-1} in the dipeptide data (Figure 4A−H).

As mentioned above, vibrational bands at 1560 and 1419 cm^{-1} are observed in spectra derived from tyrosinate (Figure 3A). However, the 1560 and 1419 cm^{-1} features are shifted to approximately 1580 and 1408 cm^{-1} in the spectra derived from tyrosine-containing dipeptides (Figure 4A−H). As discussed above, these bands have contributors assignable to tyrosinate ring stretching and/or carboxylate stretching vibrations. Therefore, these shifted frequencies constitute a significant perturbation of the tyrosinate spectrum in the dipeptides. We attribute this perturbation to changes in hydrogen bonding or to conformational changes in the tyrosine side chain, caused by peptide bond formation.

Amide I and II bands will be observed in the ground-state FT-IR spectra of the tyrosine-containing dipeptides.[38] A band at approximately 1630 cm^{-1} (Figure 4A−H) is attributed to the amide I vibration in the dipeptides. As expected, this band is not observed in tyrosinate (Figure 3A). In the tyr-pro dipeptide, which contains an imido group, the 1630 cm^{-1} band is shifted to 1679 cm^{-1} (Figure 4C).[29] The amide II band is observed at approximately 1535 cm^{-1} in the X-tyr dipeptides (Figure 4E−H), where X represents his, ile, pro, or leu. This band is not as evident in the tyr-X dipeptides (Figure 4A−D), where X represents his, ile, or leu, but may be present as a shoulder at approximately 1540 cm^{-1}. Again, as expected, the amide II band is not observed in tyr-pro dipeptide (Figure 4C) or in tyrosinate (Figure 3A). The imide group may contribute weakly to the tyr-pro spectrum at approximately 1480 cm^{-1}.[29]

Note that when the dipeptide data are compared to each other (Figure 4A−H), the vibrational spectrum in the region between 1440 and 1330 cm^{-1} is altered due to direct spectral contributions from the other side chain in the dipeptide. When each X-tyr spectrum is compared to the corresponding tyr-X spec-

(36) Chipman, D. M.; Liu, R.; Zhou, X.; Pulay, P. *J. Chem. Phys.* **1994**, *100*, 5023−5035.
(37) Bellamy, L. J. *The infrared spectra of complex molecules*; Chapman and Hall: London, 1980.
(38) Krimm, S.; Bandekar, J. *Vibrational spectroscopy and conformation of peptides, polypeptides, and proteins*; Anfinsen, C. B., Edsall, J. T., Richards, F. M., Eds.; Academic Press: New York, 1986; Vol. 38, pp 181−364.

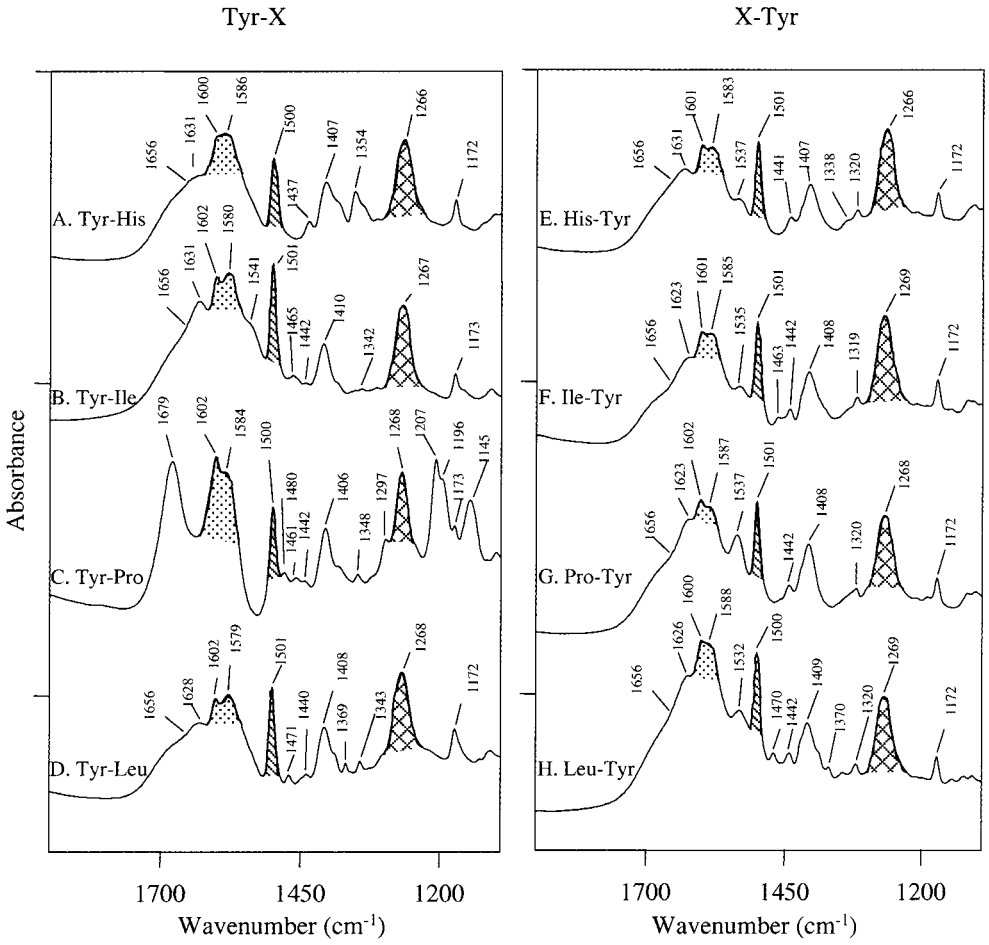

Figure 4. Ground-state FT-IR spectra of (A) tyr-his, (B) tyr-ile, (C), tyr-pro, (D) tyr-leu, (E) his-tyr, (F) ile-tyr, (G) pro-tyr, and (H) leu-tyr dipeptides. Spectral contributions from the borate buffer were subtracted from these data. The tick marks on the *y*-axis represent 1.0 absorbance units. Crosshatched lines are assigned to ring modes and the CO stretching vibrations of tyrosinate.

trum, minor perturbations are observed for the his, ile, and leu cases. These perturbations of the X-tyr spectra include an upshift of bands between 1320 and 1319 cm^{-1}, 1631 and 1623 cm^{-1} (amide I), and 1537 and 1532 cm^{-1} (amide II) in the tyr-X dipeptides. This upshift of the amide I and II bands in tyr-X peptides is consistent with a different distribution of trapped conformations[15] and/or with a different set of hydrogen bonding interactions,[13] when compared to X-tyr. In the pro-tyr and tyr-pro cases, the most dramatic changes are observed. The tyr-pro spectrum contains at least 8 bands between 1680 and 1145 cm^{-1}, which were not observed or were shifted to lower frequencies in pro-tyr. While the *trans* form of the other dipeptides is expected to be most stable in solution, in the X-pro dipeptide the *trans* isomer is destabilized relative to the *cis* form.[39] This difference in isomeric form and the absence of the amide proton may lead to differences in hydrogen bonding and thereby alter the spectrum.[13,40]

FT-IR Spectra Associated with the Photolysis Reaction in Tyrosine Solutions: ^{13}C Ring Labeling. Difference FT-IR spectroscopy was used to obtain the vibrational spectrum associated with the oxidation of tyrosinate *in vitro*. A difference infrared spectrum exhibits only those vibrations that are perturbed upon generation of the radical.[8,10,26,27,41] Data were acquired before and after UV photolysis and were manipulated in order to yield the difference spectrum. Figure 5 shows the difference FT-IR spectra acquired from borate buffer (A), tyrosinate (B), $^{13}C_1$(4′-phenol) tyrosinate (C), and ^{15}N tyrosinate (D). Positive lines in the difference FT-IR spectrum arise from the neutral tyrosyl radical, while negative lines arise from unique vibrational bands of the tyrosinate ground state. As expected, UV photolysis performed on borate buffer did not yield a difference spectrum (Figure 5A).

Perturbed tyrosinate vibrations are expected to be negative lines in the difference spectrum. In Figure 5B, negative bands are observed at 1606, 1500, 1263, and 1173 cm^{-1} and, based on our ground-state assignments, correspond to υ_{8a} (CC ring stretch), υ_{19a} (CC/CH ring stretch), $\upsilon_{7a'}$ (CO stretch), and υ_{9a} (CH bend) modes, respectively. In $^{13}C_1$(4′-phenol) tyrosinate (Figure 5C), the downshifted bands are observed at 1601, 1491, 1241, and 1172 cm^{-1}.

Because these spectra were corrected for any differences in path length and concentration, they can be directly subtracted to give an isotope-edited spectrum (Figure 5E). The only spectral contributors to the isotope-edited spectrum will be ^{13}C-sensitive bands. The isotope-edited spectrum exhibits contributions at (negative) 1609/(positive) 1600 cm^{-1}, (negative) 1501/(positive) 1490 cm^{-1}, and (negative) 1268/(positive) 1235 cm^{-1}, which

(39) Wan, S. Z.; Wang, C. X.; Wu, Y. W.; Shu, Y. Y. *Chem. Phys.* **1996**, *211*, 227−234.
(40) Ishimoto, B.; Tonan, K.; Ikawa, S. *Spectrochim. Acta, Part A* **1999**, *56*, 201−209.
(41) Berthomieu, C.; Boullais, C.; Neumann, J.-M.; Boussac, A. *Biochim. Biophys. Acta* **1998**, *1365*, 112−116.

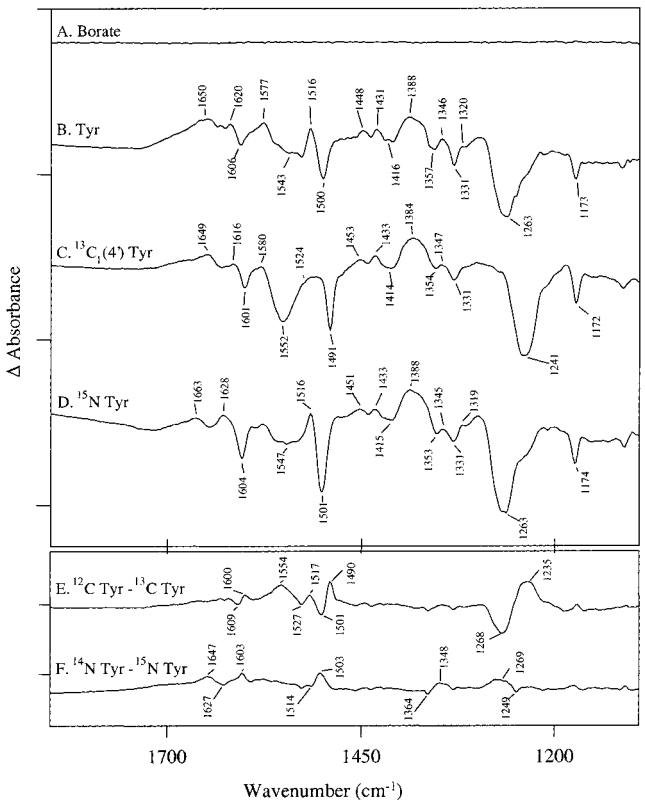

Figure 5. Difference FT-IR spectra, associated with UV photolysis, of (A) 10 mM borate buffer at pH 11, (B) tyrosyl radical-minus-tyrosinate, (C) $^{13}C_1$(4′-phenol) tyrosyl radical-minus-$^{13}C_1$(4′-phenol) tyrosinate, and (D) ^{15}N tyrosyl radical-minus-^{15}N tyrosinate. Data obtained before UV illumination were subtracted from data collected after illumination to generate these difference spectra. In (E), the double difference spectrum, ^{12}C (B)-minus-^{13}C (C), is shown. In (F), the double difference spectrum, ^{14}N (B)-minus-^{15}N (D), is shown. Tick marks on the *y*-axis represent 0.02 absorbance units.

are consistent with a significant ^{13}C-induced downshift of υ_{8a}, υ_{19a}, and $\upsilon_{7a'}$, respectively, in tyrosinate. Other negative lines at 1543, 1416, 1357, and 1331 cm^{-1} (Figure 5B) do not make a significant contribution to the ^{13}C isotope edited spectrum, probably because the ^{13}C isotope shift is small or negligible (Figure 5E). Potential assignments for these bands are discussed above.

Positive lines in the difference FT-IR spectrum arise from unique vibrational bands of the tyrosyl radical. In Figure 5B, the 1620 and 1577 cm^{-1} lines (Figure 5B) are candidates for vibrations arising from the aromatic ring. However, only a small ^{13}C isotope shift is observed for the 1620 cm^{-1} line ($\Delta = -4$ cm^{-1}) (Figure 5C,E). Because this isotope shift is smaller than the shift expected for the υ_{8a} ring stretching mode,[8,27,35,42] we assign the 1620 cm^{-1} feature to a different ring stretching vibration.

A component of the positive 1577 cm^{-1} band in Figure 5B appears to shift to 1524 cm^{-1} (shoulder) (Figure 5C). In the ^{13}C isotope-edited spectrum (Figure 5E), the positive line is observed at 1554 cm^{-1}, and we assign this band to υ_{8a}.[22,27,35,36,42] Also, a positive 1516 cm^{-1} band is observed in our tyrosine photolysis spectrum (Figure 5B). In the $^{13}C_1$(4′-phenol) tyrosinate spectrum (Figure 5C), the intensity of the 1516 cm^{-1} line decreases, and in the ^{13}C isotope-edited spectrum (Figure 5E), a positive band at 1517 cm^{-1} is shown. We assign the 1516 cm^{-1} line or a component of this line to υ_{7a} of the radical.[8,10,27,35,41,42] Note that the positions of the downshifted lines corresponding to υ_{8a} and υ_{7a} were not evident in either spectrum C or E in Figure 5, perhaps because of cancellation. Also note that in ref 41, a downshifted line was assigned to υ_{7a} in the $^{13}C_1$(4′) isotopomer. However, that result was not reproduced in our spectra, which are of higher signal-to-noise. Assignments for other positive spectral feature bands between 1500 and 1300 cm^{-1}, which do not make a significant contribution to the ^{13}C isotope-edited spectrum, will be discussed in a future publication.

FT-IR Spectra Associated with the Photolysis Reaction in Tyrosine Solutions: ^{15}N Amino Labeling. From previous work, it was expected that the oxidation spectrum will exhibit tyrosyl and tyrosinate vibrational bands, as observed above. To ascertain if there are any other contributions to the FT-IR photolysis spectrum, we carried out a photolysis experiment with ^{15}N tyrosinate (Figure 5D). The isotope-edited, ^{14}N-minus-^{15}N spectrum (Figure 5F) shows contributions at 1647/1627/1603 cm^{-1}. These bands are not observed in the isotope-edited, ^{12}C-minus-^{13}C spectrum (Figure 5E), consistent with assignment of this derivative shaped band to a $-NH_2$ deformation mode.[43,44] Such a positive/negative/positive line shape in the isotope-edited spectrum is consistent with a small ^{15}N-induced downshift of a derivative-shaped band with a positive at 1647 cm^{-1} and a negative at approximately 1627 cm^{-1}. We conclude that the oxidation reaction increases the force constant of an NH deformation mode by 2%.

Other derivative shaped spectral bands in Figure 5E may be caused by the expected ^{15}N shifts in the NH rocking, CN stretching, NH wagging, and other coupled vibrational modes.[43,44] To be consistent with the observation of simple derivative-shaped bands in the double difference data, the ^{15}N shifts for these lines must be smaller than the ^{15}N shift for the deformation mode, which shows a positive/negative/positive line shape. These results suggest an electronic interaction between the phenoxyl ring and the terminal groups of tyrosine.

Solvation Changes. A positive line between 1663 and 1649 cm^{-1} is observed in each photolysis spectrum (Figure 5B,C,D). This band may arise from the OH bending mode of water.[37] A broad combination band at approximately 2200 cm^{-1} is also observed (data not shown). These data suggest that the solvation shell is perturbed by the oxidation reaction at 77 K.

EPR Simulations with ^{14}N Couplings. The increase in force constant for the NH deformation mode may be caused by spin delocalization from the phenoxyl ring to the amino nitrogen. Spin delocalization could also cause changes in hydrogen bonding which could account for a perturbation of the solvation shell. To estimate the magnitude of this spin delocalization, we estimated the upper limit of the hyperfine coupling to the amino nitrogen.

Simulations of the tyrosyl radical spectrum were performed to test the magnitude of the axial ^{14}N hyperfine tensor[45] to ^{14}N (data not shown). The parameters employed were the same as the hyperfine splittings in Table 1, except that a hyperfine splitting to nitrogen was added to the simulation. Given the

(42) Cappuccio, J. A.; Ayala, I.; Elliot, G. I.; Szundi, I.; Lewis, J.; Konopelski, J. P.; Barry, B. A.; Einarsdottir, O. *J. Am. Chem. Soc.* **2002**, *124*, 1750−1760.
(43) Yamaguchi, A. *Nippon Kagaku Zasshi* **1959**, *80*, 1105−1109.
(44) Tsuboi, M. *Spectrochim. Acta* **1960**, *16*, 505−512.
(45) Wertz, J. E.; Bolton, J. R. *Electron spin resonance*; Chapman and Hall: New York, 1986.

Table 2. Comparison of the Spin Density Charges and Fermi Contacts for the Tyrosyl Radical Anion Calculated with Density-Functional Theory for Three Different Local Minima (I, II, and III) and a Simple Boltzmann-Weighted Average[‡]

	I		II		III		⟨average⟩	
atom	spin Q	Fermi	spin Q	Fermi	spin Q	Fermi	spin Q	Fermi
C_1	0.346	12.32	0.421	15.71	0.378	15.03	0.373	13.77
C_2/C_6	−0.163	−6.27	−0.164	−7.69	−0.146	−7.09	−0.161	−6.83
C_3/C_5	0.261	7.96	0.264	9.39	0.251	8.67	0.261	8.50
C_4	−0.040	−6.59	−0.018	−7.60	−0.015	−6.96	−0.029	−6.96
O_5	0.316	−10.64	0.352	−11.77	0.333	−11.23	0.330	−11.08
C_β	0.032	−3.34	−0.016	−4.32	0.015	−4.05	0.015	−3.75
C_α	0.002	−1.58	0.045	2.58	0.061	2.10	0.024	0.26
N	0.037	1.92	0.006	0.00	0.014	1.71	0.016	1.30
C	0.033	−2.18	−0.007	−1.01	0.001	0.43	0.024	−1.42
O_1/O_2	0.044	−1.40	0.012	−0.53	0.023	−0.68	0.031	−1.02
ring	0.818		0.956		0.904		0.873	

E	W_B	*E*	W_B	*E*	W_B	⟨*E*⟩
0	0.541	0.343	0.304	0.742	0.155	0.219

[a] Shown are the Mulliken spin density charges (spin Q) in atomic units and the Fermi contact (Fermi) in gauss. Also shown is the total spin density in the aromatic ring (ring), and the relative energies (*E*) in kcal/mol and Boltzmann weights (W_B) at 298 K. Only atoms that are distinct after conformational averaging over symmetry-equivalent structures are shown, in which case the spin density and Fermi contact are similarly averaged.

signal-to-noise, an isotropic hyperfine coupling, a_{iso}, of 0.65 G and an axial hyperfine tensor, $a_{xx} = a_{yy} = 0.49$ G and $a_{zz} = 0.98$ G, gave an indistinguishable simulation, as compared to the simulations shown in Figure 2, which did not include ^{14}N hyperfine splittings. However, when we increased the ^{14}N isotropic coupling to 1.0 G in the simulation, significant distortions of the simulated spectral lineshape were observed as compared to the data. Therefore, we estimate the size of any putative hyperfine coupling to ^{14}N as no larger than 0.65 G. In our experiments with ^{15}N tyrosine, we found that ^{15}N labeling did not significantly change the tyrosyl radical EPR spectrum (data not shown). Simulations were also performed to estimate the impact of ^{15}N labeling, given an assumed a_{iso} of 0.65 G for the ^{14}N isotopomer. These simulations were in agreement with our ^{15}N result, because they predicted that the EPR spectrum would be insensitive to ^{15}N substitution. Using the relationship, $a_{iso} = Qp$, where Q equals 23−26 G for nitrogen radicals,[45] and $a_{iso} = 0.65$ G, this analysis predicts a spin density less than 0.03 on the amino nitrogen.

DFT Calculations. DFT calculations were performed to estimate the spin density charges and Fermi contacts for symmetry distinct atoms in the neutral tyrosyl radical. The results for three optimized structures and the Boltzmann weighted average are presented in Table 2. As shown in Table 2, the distribution of spin in the tyrosyl radical exhibits considerable conformational variation. In our calculations, the range of spin density on the amino nitrogen of the tyrosyl radical was found to be between 0.006 and 0.037 (Table 2). These DFT results are consistent with a possible migration of the spin density from the phenoxyl ring to the amino nitrogen. The predicted global minimum has more spin density associated with the amino nitrogen than that of the second lowest energy structure. A full account of the theoretical work is forthcoming.

FT-IR Spectra Associated with the Photolysis Reaction in Tyrosine-Containing Dipeptides. The results above suggest an electronic interaction between the oxidized tyrosine side chain and the amino group of tyrosine. To test the idea that such an interaction occurs, the tyrosyl radical was generated in dipeptides. Figure 6 shows the difference FT-IR spectra acquired from the tyr-his (A), tyr-ile (B), tyr-pro (C), tyr-leu (D), his-tyr (E), ile-tyr (F), pro-tyr (G), and leu-tyr (H) dipeptides. The dipeptide spectra (Figure 6) exhibit negative bands at 1605−1601, 1502−1498, and 1266−1261 cm^{-1}, corresponding to tyrosinate bands υ_{8a} (CC ring stretch), υ_{19a} (CC/CH ring stretch), and $\upsilon_{7a'}$ (CO stretch) (Figure 5C). A negative line arising from the υ_{9a} (CH bend) of tyrosinate (1173−1172 cm^{-1}) was observed in each dipeptide, except for tyr-pro (Figure 6C), where it may have been canceled by a positive spectral contribution. A negative band at 1580−1563 cm^{-1} is observed, which may correspond to υ_{8b} (ring CC stretch) and/or to an asymmetric carboxylate vibrational mode. A candidate for υ_{19b} (CC stretch/CH bend) of tyrosinate is observed at 1416−1408 cm^{-1} (Figure 6A−H). Significant frequency shifts are measured when the 77 K ground state spectra and the negative bands in the photolysis spectrum are compared. This may indicate that the vibrational spectrum is altered by conformation and that a subset of frozen conformations is preferentially oxidized.[25]

The difference infrared spectra of tyrosine-containing dipeptides (Figure 6A−H) also exhibit a positive band between 1510 and 1515 cm^{-1}. This line or a component of this line may be assigned to the CO stretching vibration (υ_{7a}) of the tyrosyl radical in the dipeptides. Note that there are significant shifts (5 cm^{-1}) in the frequency of this vibrational mode in different dipeptides and that these frequency shifts are dipeptide dependent {compare, for example, tyr-leu (Figure 6D) and leu-tyr (Figure 6H)}. To summarize these results, the most perturbed vibrational bands, when comparing the dipeptide photolysis data to the tyrosinate data, are the υ_{7a} CO stretch and putative ring stretching/carboxylate bands at 1580−1563 and 1416−1408 cm^{-1}, respectively.

The dipeptide spectra (Figure 6) also show unique vibrational bands, when compared to tyrosinate (Figure 5). Tyrosine-containing dipeptides with sequence X-tyr, where X is his, ile, pro, or leu, exhibited a derivative-shaped feature with a negative band between 1536 and 1531 cm^{-1} and a positive band between 1554 and 1543 cm^{-1} (Figure 6E−H). On the basis of our assignments of the ground-state spectra, this band is attributed to an oxidation-induced perturbation of the amide II vibration. The negative band at 1628−1621 cm^{-1} in dipeptides with sequence X-tyr (Figure 6E−H) may be attributable to the amide I band. These bands were not as evident in the tyr-X dipeptides (Figure 6A−D), except that tyr-pro exhibited a spectral con-

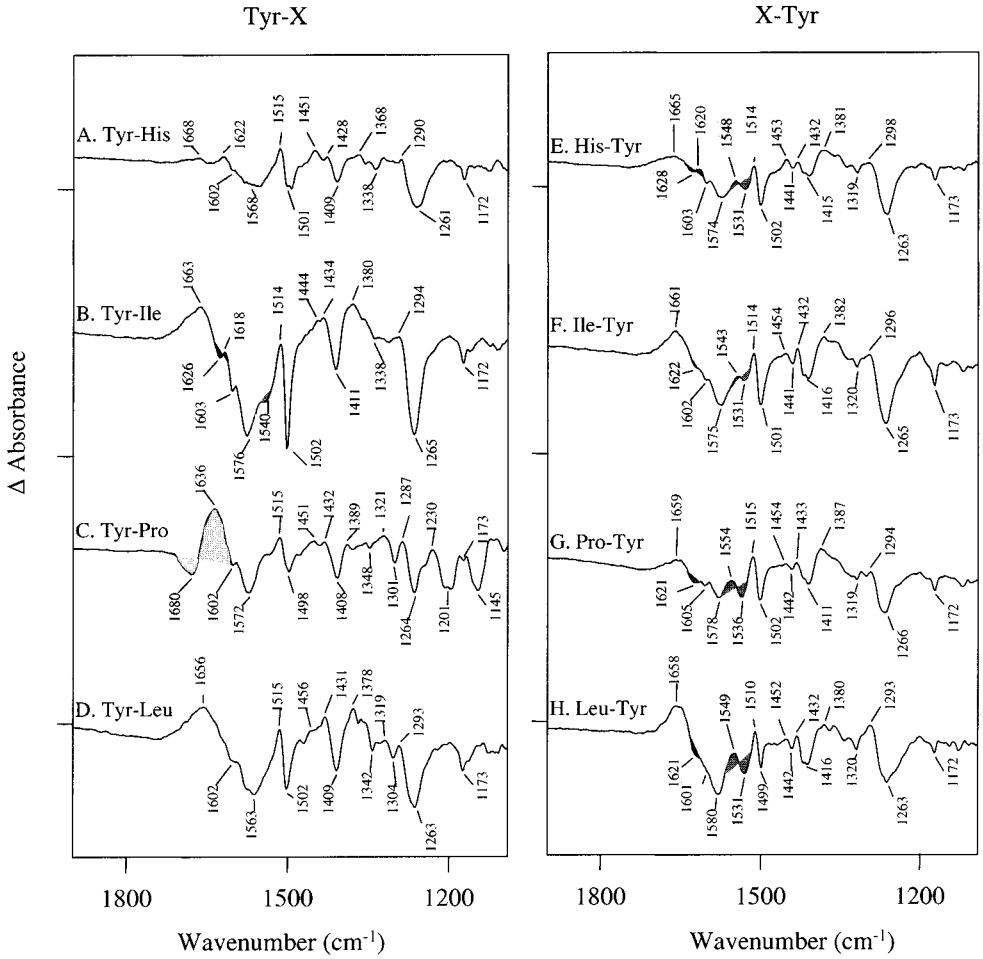

Figure 6. Difference FT-IR spectra, associated with UV photolysis, of (A) tyrosyl radical histidine-minus-tyrosinate-histidine, (B) tyrosyl radical isoleucine-minus-tyrosinate-isoleucine, (C) tyrosyl radical proline-minus-tyrosinate-proline, (D) tyrosyl radical-leucine-minus-tyrosinate-leucine, (E) histidine-tyrosyl radical-minus-histidine-tyrosinate, (F) isoleucine-tyrosyl radical-minus-isoleucine-tyrosinate, (G) proline-tyrosyl radical-minus-proline-tyrosinate, and (H) leucine-tyrosyl radical-minus-leucine tyrosinate. Data obtained before UV illumination were subtracted from data collected after illumination to generate these difference spectra. Tick marks on the *y*-axis represent 0.04 absorbance units. Crosshatched bands denote bands assigned to amide I or amide II vibrational modes.

tribution at 1680/1636 cm^{-1} that may arise from amide I (Figure 6C). As expected, tyr-pro, which contains an imide linkage, did not show evidence of an amide II contribution (Figure 6C). Amide I and II band contributions may have been observed in the tyr-ile dipeptide (Figure 6B), but were not evident in the tyr-his and tyr-leu peptides (Figure 6A,D).

In the case of tyr-pro, unique vibrational bands were observed that are not found in the pro-tyr spectrum (compare spectra C and G in Figure 6). The tyr-pro and pro-tyr dipeptides differ in the distribution of *trans* and *cis* conformers in solution. Therefore, we assign unique bands in the tyr-pro spectrum to an oxidation-induced, conformationally dependent perturbation of the pro group.

Discussion

In this report, we have generated tyrosyl radicals by UV photolysis and studied the structure of these paramagnetic species through EPR and infrared spectroscopies. EPR is sensitive to the unpaired electron spin density in the radical and to the single bond conformation at $C_\beta-C_1$ (Figure 1A). The vibrational spectrum will reflect conformation as well as changes in the distribution of total electron density throughout the molecule. Although the structure of the radical produced by pulse radiolysis and by photolysis has been studied by EPR and vibrational techniques, the impact of peptide bond formation has not been investigated previously.

In tyrosinate solutions and in tyrosine-containing dipeptides, a radical was generated by photolysis and was detected by EPR spectroscopy. The measured isotropic *g* value and the spectral line width of the radicals produced in dipeptides and in solution were similar to each other and were similar to EPR signals previously attributed to neutral tyrosyl radicals.[11,12] An EPR spectrum, with a broadened line shape, was obtained for the $^{13}C_1$(4′-phenol) isotopomer of tyrosine. The spectral line shape of the isotopomer was reproduced with parameters used to simulate the tyrosine spectrum, when an additional hyperfine splitting to the ^{13}C nucleus was included in the simulation. The radical formed in the tyr-pro dipeptide had the most perturbed EPR line shape of the dipeptides examined. This spectrum could be simulated by modifying the β-methylene hyperfine couplings; the change was consistent with a 9° rotation at the $C_\beta-C_1'$ bond (Figure 1A). These changes are attributed to the presence of an imide linkage to proline, which alters the stability of the *cis*/*trans* forms of the dipeptides and thereby causes other conformational changes in the dipeptide.[39] This work demonstrates that a neutral tyrosyl radical is generated by photolysis in the

dipeptides.[21] We also used simulations to estimate the maximum value of any hyperfine coupling to the amino ^{14}N in tyrosine. The isotropic hyperfine splitting, a_{iso}, obtained had an upper limit of 0.65 G and the maximum value of any spin density on the nitrogen was estimated as 0.03.

Reaction-induced FT-IR spectroscopy has the potential to give additional structural information about the radical and its intramolecular interactions.[46] Previous vibrational studies have shown that aromatic ring stretching vibrations and the CO stretching vibration of tyrosinate are perturbed by oxidation of the aromatic ring.[8] The CO vibration is expected to upshift by 300 cm^{-1} upon formation of the neutral radical. This upshift has been explained as a delocalization of the unpaired electron onto the phenol oxygen in the neutral radical.[8] If there is coupling between the oxidation reaction and other structural changes in the molecule, the reaction-induced FT-IR spectrum will reflect those structural changes, as well as the structural changes of the tyrosinate side chain.

Accordingly, reaction-induced FT-IR spectra, associated with the photolysis of tyrosinate and dipeptides, were acquired. Use of an isotopomer of tyrosinate, $^{13}C_1$(4′-phenol) tyrosine, allowed bands to be assigned to the phenyl ring of tyrosinate and of the tyrosyl radical. ^{15}N labeling of the amino group of tyrosine demonstrated that the photolysis spectrum exhibits a contribution from NH bending and other N-sensitive modes. This ^{15}N result suggests that the electronic structure of the tyrosine amino group is perturbed by the oxidation reaction. Radical formation resulted in an upshift of the NH deformation, consistent with a 2% increase in force constant. This change in force constant may, in turn, reflect spin delocalization onto the nitrogen. DFT calculations provided support for this interpretation and predicted that spin density delocalizes onto the amino and carboxylate groups of the tyrosyl radical.

To test the idea of an electronic interaction between the radical and other functional groups in the molecule, the tyrosyl radical was then generated in dipeptides, and the reaction induced FT-IR spectrum was obtained. We postulated that if an interaction occurred between the amino group and tyrosyl radical, amide spectral contributions might be detected in dipeptides. Dipeptides are a good material for this investigation, because there is no transition dipole coupling,[16,38] allowing the amide region of the spectrum to be interpreted more easily. In all the X-tyr dipeptides examined, the oxidation reaction resulted in an amide II contribution to the photolysis spectrum. A less intense amide I contribution, of opposite sign, was also observed. The tyr-X peptides had either no detectable or a much less intense amide II contribution to the photolysis spectrum. An amide I contribution was also observed in the tyr-pro peptide; the imide vibrational mode is not very intense in this molecule and would not be detectable. However, the photolysis spectrum obtained on tyr-pro exhibited unique vibrational bands, suggesting an oxidation-induced perturbation of vibrational modes of the proline side chain.

The lower intensity of the amide II contribution in the tyr-X peptides may be due to the fact that the amide II band was overlapping with aromatic stretching vibrations in the infrared absorption spectra of these peptides (Figure 4). Alternatively, the lower intensity in tyr-X can be explained if spin delocalization occurs by a through-bond mechanism. Finally, if the spin delocalization occurs by a through-space mechanism, as previously proposed,[30] the intensity difference can be explained by a difference in average distance between the tyrosine ring and the amide nitrogen in the two classes of dipeptides.

As additional support for the hypothesis that an electronic interaction occurs between the radical and the amine or amide group, tyrosyl radical vibrational frequencies were observed to be altered in the dipeptides, when compared to tyrosinate. This is significant and suggests an intramolecular effect, because the radical is generated at 77 K from the diamagnetic distribution of conformations and because large conformational rearrangement is precluded at this temperature.[25] As an example, the frequency of the radical CO stretching mode varied by 5 cm^{-1} when tyr-leu and leu-tyr were compared. However, the CO stretching frequency of the ground-state molecule was the same in these two dipeptides. We speculate that these frequency perturbations of the dipeptide tyrosyl vibrational modes are caused by an interaction between the radical and other functional groups, including the amide nitrogen. Because such an interaction is predicted to depend on conformation{see Table 2 and ref 30}, the magnitude of the interaction should be sequence dependent. This was observed in our data.

Previous quantitation of the spin density delocalized in the tyrosyl aromatic ring has given numbers close to one.[12,47] Therefore, if spin delocalization underlies the change in force constant, the amount of spin density delocalized onto the amine nitrogen must be small. As assessed from our EPR data and spectral simulations, the upper limit for this value is 0.03. DFT calculations, which predicted a N spin density of 0.02 in the Boltzmann-weighted average, are in good agreement with this experimentally derived limit.

Spin density "charges" are not real observables, and depend on the partitioning technique that is used. The Mulliken partition scheme that was used here, as in the other studies,[35,48] is sensitive to basis set. Consequently, direct comparison of numbers obtained from different methods and basis sets is not straightforward. However, the spin density distribution in Table 2 is qualitatively similar to values recently reported. The largest discrepancy is in the density at the phenol oxygen. Recent experimentally reported values for this spin density are between 0.28 and 0.27.[12,47] Calculations using a semiempirical AM1 model[48] reported a spin density of 0.17 at the phenol oxygen. Qin and Wheeler,[35] using density functional methods with the local spin density exchange functional of Slater[49] and the correlation functional of Vosko, Wilk, and Nusair (SVWN),[50] reported a value of 0.36. The latter spin density is similar to the Boltzmann average value of 0.33 reported here (Table 2).

In addition to spin polarization, other possible interactions that could account for a change in the force constant of the NH bending mode are a conformational rearrangement, a change in intramolecular hydrogen bonding, or a solvation change. Intermolecular interactions are unlikely at the concentrations employed here. Previous work has shown distortion of the phenol photolysis spectrum at very high concentrations (1 M) due to intermolecular interactions;[41] this type of distortion is

(46) Kim, S.; Barry, B. A. *J. Phys. Chem. B* **2001**, *105*, 4072−4083.
(47) Dole, F.; Diner, B. A.; Hoganson, C. W.; Babcock, G. T.; Britt, R. D. *J. Am. Chem. Soc.* **1997**, *119*, 11540−11541.
(48) O'Malley, P. J.; MacFarlane, A. J.; Rigby, S. E. J.; Nugent, J. H. A. *Biochim. Biophys. Acta* **1995**, *1232*, 175−179.
(49) Slater, J. C. In *Quantum Theory of Molecules and Solids*; McGraw-Hill: New York, 1974; Vol. 4, pp 12−55.
(50) Vosko, S. H.; Wilk, L.; Nusair, M. *Can. J. Phys.* **1980**, *58*, 1200−1211.

not observed in our data. Intramolecular hydrogen bonding between the tyrosinate side chain and the amino/amide group seems unlikely, given steric constraints. While we cannot completely exclude the possibilities of conformational rearrangement and solvation changes, if they occur at 77 K, these changes must be subtle. Note that a spin delocalization mechanism could itself lead to small changes in solvation and conformation by causing changes in hydrogen bonding. Indeed, effects of tyrosine oxidation on the solvation shell were observed in our FT-IR photolysis spectra.

To summarize our results, we have examined the vibrational and EPR spectra of tyrosyl radicals produced in polycrystalline tyrosinate and tyrosine-containing dipeptides. This work has provided evidence for significant, sequence-dependent alterations in conformation and hydrogen bonding, which in turn lead to spectroscopic alterations. We have also presented evidence for a migration of unpaired spin density from the phenoxyl ring to terminal groups. This was detected by difference FT-IR spectroscopy as a change in force constant for the NH deformation mode in tyrosinate or for the amide II vibration in X-tyr dipeptides. Finally, DFT calculations have allowed us to estimate the spin density at the terminal amino and carboxylate groups of the tyrosyl radical.

In photosystem II, there are two redox active tyrosines, D and Z, with different functional roles in the enzyme.[51] The location of Z and D in the primary sequence has been identified by site-directed mutagenesis {reviewed in ref 51}. These tyrosines are flanked by isoleucine and proline residues.[52] To model the PSII tyrosyl radicals, we selected tyrosine-containing dipeptides based on this sequence.

Previous work on tyrosyl radicals in PSII has shown that there are significant frequency shifts of tyrosyl radical vibrational modes in this protein.[53−55] These results have been recently reviewed.[55] ^{15}N-sensitive vibrational bands were observed in the amide II region of these PSII tyrosyl radical spectra.[53] Some of those vibrational modes may arise from the tyrosine amide nitrogen. ESEEM studies have also provided evidence for coupling to a peptide nitrogen in the environment of tyrosine D.[56]

The work reported here predicts that oxidation of tyrosine will be accompanied by additional perturbations to other functional groups, especially the peptide moiety, in proteins. These conclusions may also have important implications concerning electron-transfer pathways in proteins. This work provides a step in a systematic examination of the effects of polarity, hydrogen bonding, electrostatics, and conformation on the structural and functional properties of redox-active tyrosines.

Acknowledgment. This work was supported by NIH GM 19541 (I.A.), NIH GM 43273 (B.A.B.), and NIH GM 62248 (D.Y.). The authors are grateful for computational resources provided by the Minnesota Supercomputing Institute and thank Prof. Sunyoung Kim (Virginia Tech) and Dr. Bengt Svensson for helpful discussions.

JA0164327

(51) Barry, B. A. *Methods Enzymol.* **1995**, *258*, 303−319.
(52) Svensson, B.; Vass, I.; Styring, S. *Z. Naturforsch.* **1991**, *46c*, 765−776.
(53) Kim, S.; Barry, B. A. *Biophys. J.* **1998**, *74*, 2588−2600.
(54) Ayala, I.; Kim, S.; Barry, B. A. *Biophys. J.* **1999**, *77*, 2137−2144. Kim, S.; Patzlaff, J. S.; Krick, T.; Ayala, I.; Sachs, R. K.; Barry, B. A. *J. Phys. Chem. B* **2000**, *104*, 9720−9727.
(55) Kim, S.; Barry, B. A. *J. Phys. Chem. B* **2001**, *105*, 4072−4083.
(56) Campbell, K. A.; Peloquin, J. M.; Diner, B. A.; Tang, X.-S.; Chisholm, D. A.; Britt, R. D. *J. Am. Chem. Soc.* **1997**, *119*, 4787−4788.